https://doi.org/10.5194/acp-2019-945
Preprint. Discussion started: 23 October 2019
© Author(s) 2019. CC BY 4.0 License.

Atmospheric Chemistry and Physics Discussions

Role of ammonia on fine-particle pH in agricultural regions of China: Comparison between urban and rural sites

Shenbo Wang [a], Lingling Wang [b], Yuqing Li [c], Chen Wang [a], Weisi Wang [b], Shasha Yin [a, *], Ruiqin Zhang [a, *]

[a] *Research Institute of Environmental Science, College of Chemistry, Zhengzhou University, Zhengzhou, 450001, China*

[b] *Department of Environmental Protection of Henan Province, Zhengzhou, 450001, China*

[c] *Department of Environment Science and Engineering, Tsinghua University, Beijing 100084, China*

* Corresponding authors：Shasha Yin and Ruiqin Zhang

E-mail addresses: shashayin@zzu.edu.cn；rqzhang@zzu.edu.cn

https://doi.org/10.5194/acp-2019-945
Preprint. Discussion started: 23 October 2019
© Author(s) 2019. CC BY 4.0 License.

Atmospheric Chemistry and Physics Discussions

Abstract: Particle acidity is a fundamental property that affects atmospheric particulate chemistry. Synchronous online monitoring was performed in two urban sites (e.g., Zhengzhou (U-ZZ) and Anyang (U-AY)) and three rural sites (e.g., Anyang (R-AY), Xinxiang (R-XX), and Puyang (R-PY)) in Henan Province during a haze episode to investigate the pH value and its driving factors in the agricultural regions of China. The pH values of particles calculated by ISORROPIA-II model at rural sites were slightly higher than those urban sites, with the median values in the order of 5.2 (4.8–6.9, R-PY) > 5.1 (4.7–6.5, R-AY) > 4.9 (4.1–6.8, R-XX)> 4.8 (3.9–5.9, U-AY)> 4.5 (3.8–5.2, U-ZZ). Sensitivity tests showed that excess ammonia mainly affected the pH value of $PM_{2.5}$. Moreover, low ammonia determined the high sensitivities of particle pH to sulfate and nitrate at urban sites. Elevated sulfate and nitrate in aerosol caused high pH sensitivity to ammonia. Regional transport may enhance the particle pH value in urban aerosols given the high pH of particles and high ammonia levels in rural and agricultural regions. These results suggest that ammonia is urgently needed to be involved in the regional strategy for the improvement of air quality in China.

Keywords: ISORROPIA-II model, Particle acidity, Sulfate, Ammonia, Sensitivity test.

1 Introduction

High concentrations of acids and bases contained in the aqueous phase define the acidity of aerosols (Spurny, 1990). Particle acidity or pH value is an important parameter for atmospheric particulate chemistry, such as the gas-particle portioning of semi-volatile and volatile species (e.g., NH_3/NH_4^+, HCl/Cl^-, and HNO_3/NO_3^-), the formation of secondary inorganic and organic aerosols, and the dissolution of metallic element (Bougiatioti et al., 2016; Meskhidze et al., 2003; Seinfeld and

https://doi.org/10.5194/acp-2019-945
Preprint. Discussion started: 23 October 2019
© Author(s) 2019. CC BY 4.0 License.

Atmospheric Chemistry and Physics Discussions

Pandis, 2006; Shi et al., 2019; Shi et al., 2010; Surratt et al., 2010; Wang et al., 2018b). Particle acidity can affect the ecosystem through its influence on wet/dry deposition, atmospheric visibility, and radiative balance (Boucher and Anderson, 1995; Larssen et al., 2006; Watson, 2002). In addition, high particle acidity has an adverse impact on public health, especially for the cardiopulmonary and respiration system of humans (Dockery et al., 1996; Ostro et al., 1991).

Direct measurements on particle pH are challenging because of the small size and nonideality of chemical species in solvated aerosols. Therefore, thermodynamic models, such as E-AIM (http://www.aim.env.uea.ac.uk/aim/aim.php) and ISORROPIA-II (http://isorropia.eas.gatech.edu) (Clegg et al., 1998; Nenes et al., 1998), which rely on the measurements of particulate and gaseous species, are widely used in estimating particle pH. Table 1 shows that the fine particulate matter with an aerodynamic diameter ≤ 2.5 μm ($PM_{2.5}$) in mainland China were moderately acidic with pH values that ranged from 3.4–5.7 (Ding et al., 2019; Guo et al., 2017; Liu et al., 2017; Shi et al., 2017, 2019; Song et al., 2018; Wang et al., 2019a). Moreover, these results are 3–5 units higher than those reported in other regions, such as Hong Kong (0.25), Singapore (0.6), USA (0.07 ± 0.96 and 1.94 ± 0.59), and Greece (1.25 ± 1.14) (Behera et al., 2013; Bougiatioti et al., 2016; Guo et al., 2016; Guo et al., 2014; Pathak et al., 2004). High atmospheric total ammonia (TNH_x, gas NH_3 plus particle NH_4^+) is a dominant factor that affects the high pH values in megacities of China because it suppresses the production of particle hydronium (Cheng et al., 2016; Wang et al., 2016). The primary sources for ammonia include agricultural emissions, such as livestock waste, N-fertilizer application, and biomass burning, as well as traffic and industrial emissions (Huang et al., 2012; Shen et al., 2011; Wang et al., 2018a). According to field studies, high concentrations of NH_3 and NH_4^+ were found at rural sites in

https://doi.org/10.5194/acp-2019-945
Preprint. Discussion started: 23 October 2019
© Author(s) 2019. CC BY 4.0 License.

Atmospheric Chemistry and Physics Discussions

64 the North China Plain (Meng et al., 2011; Meng et al., 2017; Shen et al., 2011; Wen et al., 2015).
65 Therefore, studying in an agriculturally developed region is needed to obtain insight into the role of
66 ammonia in particle pH. Unfortunately, previous studies mainly concentrated on calculating the
67 particle pH in the megacity of China, and only few studies focused on the agricultural regions of China.
68 In addition to ammonia, particle pH can be influenced by chemical compositions and
69 meteorological conditions, such as aerosol water content (AWC), sulfate, temperature (T), and relative
70 humidity (RH). Liu et al. (2017) argued that excessive NH_3 and elevated AWC were responsible for
71 the high pH in Beijing. Nevertheless, Guo et al. (2017) and Song et al. (2018) demonstrated that high
72 levels of ammonia did not increase the $PM_{2.5}$ pH into a fully neutralized condition in Beijing and Xi'an,
73 China. Sensitivity tests in Beijing also suggested that sulfate, TNH_x, and T were the common driving
74 factors, and Ca^{2+} and RH were the unique factors in special seasons (Ding et al., 2019). The pH
75 sensitivity based on the 10-year record in Canada showed that chemical compositions had various
76 effects on particle pH under different meteorological conditions; moreover, careful examination for
77 any particular region is needed (Tao and Murphy, 2019).
78 Henan Province is situated in Central China; it has a dense rural population and is a top-ranking
79 province in China in terms of agricultural production and chemical fertilizer consumption (NBS, 2016).
80 NH_3 emission inventory for Henan Province reported that approximately 1031.6 Gg NH_3 was released
81 in Henan in 2015, thereby contributing to approximately 10% of China's total emissions
82 (approximately 10 Tg) (Huang et al., 2012; Wang et al., 2018a). Livestock waste and N fertilizer
83 application were major sources for ammonia emissions, which may increase TNH_x concentrations at
84 rural sites than in urban sites. Furthermore, Henan Province is a severely $PM_{2.5}$-polluted region in

https://doi.org/10.5194/acp-2019-945
Preprint. Discussion started: 23 October 2019
© Author(s) 2019. CC BY 4.0 License.

Atmospheric Chemistry and Physics Discussions

China. In January 2018, a large-scale and long-lasting haze episode that caused $PM_{2.5}$ concentration to reach 400 μg/m^3 occurred in this region (Wang et al., 2019c). An experiment was performed in two urban and three rural sites in Henan Province to investigate the pH values and their driving factors in this region. ISORROPIA-II was utilized to estimate the pH of $PM_{2.5}$ using a high time-resolution dataset. The novelty of the work addressed in the present study is that this study is the first on particle pH by comparing urban and rural sites in the agricultural regions of China. The specific objectives of the study were presented as follows: (1) Estimation and comparison of the $PM_{2.5}$ pH at the five monitoring sites, (2) identification of the factors that determine the pH, and (3) discussion of the factors that affect the different sensitivities of pH to the chemical composition in the five sites. Our results are helpful to understand the factors that determine particle acidity better.

2 Experiment and methods

2.1 Site descriptions

Field sampling was conducted from January 12 to 24, 2018 synchronously at five sites (i.e., two urban sites located in the center of Zhengzhou (U-ZZ) and Anyang (U-AY), and three sites located in the rural areas of Anyang (R-AY), Xinxiang (R-XX), and Puyang (R-PY)). Locations of the five sites with brief descriptions are listed in Table 2. U-ZZ site is surrounded by busy roads, and two freeways are located 3 km to the south and 7 km to the east. In addition, this site is near a coal-fired power plant; a gas-fired power plant; and several small-scale industries, such as pharmaceutical, electron, and equipment manufacturing. U-AY site is surrounded by busy roads, and Anyang steelwork is located 8 km to the west. R-AY site is surrounded by farmland and is 1 km west of the Jing-Gang-Ao freeway and 1 km north of a belt freeway. R-XX and R-PY sites are surrounded by farmland without other

https://doi.org/10.5194/acp-2019-945
Preprint. Discussion started: 23 October 2019
© Author(s) 2019. CC BY 4.0 License.

Atmospheric Chemistry and Physics Discussions

106 prominent anthropogenic emission sources.

107 **2.2 Instrumentations**

108 The hourly mass concentrations of water-soluble inorganic ions (WSIIs) in $PM_{2.5}$, such as NH_4^+,
109 SO_4^{2-}, NO_3^-, Cl^-, Na^+, Mg^{2+}, Ca^{2+}, and K^+ and their gaseous precursors (i.e., NH_3, HNO_3 and HCl)
110 were measured using an ambient ion monitor (URG-9000D, Thermal Fisher Scientific, USA) in U-ZZ
111 site and the monitor for aerosols and gases (MARGA, Metrohm, Switzerland) in four other sites. Both
112 instruments are successfully deployed in several other field experiments using the similar analytical
113 method (Li et al., 2017; Shi et al., 2017; Wang 2019b), and detailed information is available elsewhere
114 (Markovic et al., 2012; Rumsey et al., 2013). As a brief summary, ambient air is drawn into the systems
115 at a flow rate of 16.7 L/min. Subsequently, particles and gases are collected by two aerosol sample
116 collectors through a wet parallel plate or wet rotating denuder. Aqueous solution samples are quantified
117 by using two ion chromatography analyzers. The detection limits of five instruments for 11 species
118 during the sampling periods were less than 0.1 μg/m^3. Hourly elemental carbon (EC) and organic
119 carbon (OC) concentrations in $PM_{2.5}$ determined by the semi-continuous carbon analyzers (Model 4,
120 Sunset Laboratory Inc, USA) were obtained at the same place and time, except for the U-ZZ site, of
121 which data were provided by the Department of Environmental Protection of Henan Province. Detailed
122 information on this instrument can be found in Panteliadis et al. (2014). The OC and EC collected by
123 the device were oxidized to carbon dioxide and analyzed by a nondispersive infrared detector.
124 Meteorological parameters, including T, RH, wind direction, and wind speed were recorded
125 simultaneously at the same site.

https://doi.org/10.5194/acp-2019-945
Preprint. Discussion started: 23 October 2019
© Author(s) 2019. CC BY 4.0 License.

Atmospheric Chemistry and Physics Discussions

126 **2.3 pH prediction**

127 The pH values of $PM_{2.5}$ were estimated using the ISORROPIA-II thermodynamic model. Input
128 data, including WSIIs, gaseous precursors, RH, and T, were used to calculate the particle hydronium
129 ion concentration per volume of air (H^+_{air}) and particle water associated with inorganics (AWC_{inorg}) by
130 computing the equilibrium composition for the Na^+-K^+-Ca^{2+}-Mg^{2+}-NH_4^+-SO_4^{2-}-NO_3^--Cl^--H_2O
131 aerosol system. Considering that forward mode is less sensitive to measurement error than the reverse
132 mode and high RH levels were recorded in sampling periods, ISORROPIA-II was run in the forward
133 model for the aerosol system in the metastable condition (Ding et al, 2019). Aerosol pH was calculated
134 according to the formula (Bougiatioti et al., 2016):

135 $$\mathrm{pH} = -\log_{10} H^+_{aq} = -\log_{10} \frac{1000 H^+_{air}}{AWC_{inorg} + AWC_{org}}, \quad (1)$$

136 where the modeled concentrations for AWC_{inorg} and H^+_{air} are μg/m^3, and AWC_{org} is the particle water
137 associated with the organics predicted using the method:

138 $$AWC_{org} = \frac{m_s}{\rho_s} \frac{k_{org}}{\left(\frac{1}{\mathrm{RH}} - 1\right)}, \quad (2)$$

139 where m_s is the mass concentrations of organic matter (OC×1.6), ρ_s is the organic density (1.35
140 g/cm^3), and k_{org} is the organic hygroscopicity parameter (0.06) (Liu et al., 2017).

141 The reliability of pH calculation depends on several assumptions, such as the equilibrated gas and
142 particle phases. Thus, the predicted and observed semi-volatile species (e.g., NH_4^+, SO_4^{2-}, NO_3^-, NH_3,
143 HNO_3, and HCl) were compared to evaluate the reliability of the calculated pH. Prior this step, good
144 ion balances (Text S1 for more details of calculation) for input WSIIs were observed with an average
145 equivalent ratio that ranged from 0.99 ± 0.13 (U-ZZ) to 1.20 ± 0.12 (R-AY) in this work, thereby

https://doi.org/10.5194/acp-2019-945
Preprint. Discussion started: 23 October 2019
© Author(s) 2019. CC BY 4.0 License.

Atmospheric Chemistry and Physics Discussions

146 assuring the validity and quality of input data. Figure S2 shows that the observed and predicted NH_4^+,
147 SO_4^{2-}, and NO_3^- exhibit significant correlations, have correlation coefficients (r) above 0.99, and have
148 slopes near 1 at the five sites. In addition, NH_3 was also in good agreement with r values between 0.83
149 (U-ZZ) and 0.99 (U-AY and U-XX) and slopes between 0.80 (U-ZZ) and 1.23 (R-PY). These results
150 suggest the good performance of ISORROPIA-II when modeling these species. However, the
151 correlations between predicted and observed HNO_3 and HCl are weak. This result is similar to other
152 reported studies because of low gas concentrations, the distraction of coarse-mode particles, or
153 instrument error (Ding et al., 2019, Liu et al., 2017). Furthermore, the $PM_{2.5}$ pH was also calculated
154 by E-AIM (Version IV) to evaluate the performance of ISORROPIA-II using the observed data (RH >
155 60%) in the U-ZZ site as an example. Close correlation (r = 0.89) is observed between two models
156 with a slope of 0.95 (Fig. S3). The pH values in ISORROPIA-II are 0.46 ± 0.15 units higher than those
157 in E-AIM. These values are comparable to the results found in Liu et al. (2017) and Song et al. (2018).
158 Therefore, the predicted pH values using ISORROPIA-II are effective in this work.

159 **2.4 NH_x calculation**

160 TNH_x, required NH_x (Required-NH_x), and excess NH_x (Excess-NH_x) concentrations were
161 calculated using the following formulas:

162 $$\text{Total } NH_x = 17 \times \left(\frac{[NH_4^+]}{18} + \frac{[NH_3]}{17}\right), \quad (3)$$

163 $$\text{Required } NH_x = 17 \times \left(\frac{[SO_4^{2-}]}{48} + \frac{[NO_3^-]}{63} + \frac{[Cl^-]}{35.5} + \frac{[HNO_3]}{64} + \frac{[HCl]}{36.5}\right) - 17 \times \left(\frac{[Na^+]}{23} + \frac{[K^+]}{39} + \frac{[Ca^{2+}]}{20} + \frac{[Mg^{2+}]}{12}\right), \quad (4)$$

164 $$\text{Excess } NH_x = \text{total } NH_x - \text{required } NH_x, \quad (5)$$

https://doi.org/10.5194/acp-2019-945
Preprint. Discussion started: 23 October 2019
© Author(s) 2019. CC BY 4.0 License.

Atmospheric Chemistry and Physics Discussions

where [Na^+], [K^+], [Ca^{2+}], [Mg^{2+}], [NH_4^+], [SO_4^{2-}], [NO_3^-], [Cl^-], [NH_3], [HNO_3], and [HCl] are the measured mass concentrations ($\mu g/m^3$) of these species. If excess NH_x is above 0, then the system is considered NH_x-rich. Otherwise, the system is under the NH_x-poor condition.

3 Results and discussion

3.1 Haze episodes

During the sampling periods, five monitoring sites simultaneously experienced a long-lasting and large-scale haze episode. Time series of the concentrations of WSIIs, NH_3, and meteorological parameters are presented in Fig. 1 at the U-ZZ site as an example, and other sites are shown in Fig S4, with the mean values listed in Table 3. Three study cases were classified on the basis of the meteorological conditions and chemical component levels. The concentrations of WSIIs at five sites during Case 1 (January 12−14) gradually increased with T and RH in the southern wind. Elevated concentrations of WSIIs during Case 2 (January 14–21) were under high T and RH conditions with variable wind directions. Case 3 (January 21–25) was characterized by decreased pollutant concentrations, T, and RH with the northern wind. Evidently, the back trajectory frequency analysis (Figs. S5a and c) shows that the chemical components of $PM_{2.5}$ at the five sites in Cases 1 and 3 were predominantly influenced by the southern and northern air mass transport, respectively. In contrast, local emissions played a key role in the pollution levels during Case 2 (Fig. S5b).

Even though the total WSIIs concentrations were comparable, the chemical components of WSIIs under the effects of air masses from opposite directions were distinctly different between Cases 1 and 3. NO_3^-, NH_4^+, and NH_3 concentrations in Case 1 were higher than those in Case 3 at all sites. However, the SO_4^{2-} concentrations in Case 1 were lower than those in Case 3 (Table 3). Wang et al. (2018a)

https://doi.org/10.5194/acp-2019-945
Preprint. Discussion started: 23 October 2019
© Author(s) 2019. CC BY 4.0 License.

Atmospheric Chemistry and Physics Discussions

reported that southern cities of Henan Province (e.g., Nanyang, Shangqiu, Zhoukou, and Zhumadian) had relatively higher ammonia emissions than the cities involved in this study. Moreover, the northern air masses from the Jing–Jin–Ji regions were easily enriched with sulfate (Wang et al., 2019b; Wang et al., 2018c). The concentrations of chemical composition under stagnant weather conditions in Case 2 clearly increased with average NH_4^+, SO_4^{2-}, and NO_3^- concentrations that ranged from 12.8 ± 4.5 μg/m^3 (U-ZZ) to 45.5 ± 13.6 μg/m^3 (R-AY), 30.9 ± 13.4 μg/m^3 (R-XX) to 44.1 ± 17.5 μg/m^3 (R-AY), and 56.6 ± 19 μg/m^3 (U-AY) to 74.5 ± 20.7 μg/m^3 (R-AY). The order of average concentrations of each WSIIs at the five sites varied substantially, but the average concentrations of NH_3 at rural sites were higher than those at urban sites in the order of R-PY (26.5 ± 6.7 μg/m^3) > R-XX (25.1 ± 10.0 μg/m^3) > R-AY (25.0 ± 6.7 μg/m^3) > U-AY (23.1 ± 6.6 μg/m^3) > U-ZZ (19.0 ± 5.3 μg/m^3). Moreover, the NH_3 levels in this work were extremely higher than the NH_3 concentrations used in predicting pH values in Beijing (12.8 μg/m^3) and Xi'an (17.3 μg/m^3) (Guo et al., 2017), as well as other studies summarized in Table S1. Agricultural emissions, including livestock waste, N fertilizer application, and humans, were the top three ammonia contributors in Henan Province (Wang et al., 2018a), which may result in high ammonia concentrations at rural sites during Case 2.

3.2 pH of $PM_{2.5}$ at the urban and rural sites

Figure 2 exhibits the predicted $PM_{2.5}$ pH values, H^+_{air}, and AWC at the five sites. $PM_{2.5}$ have consistent moderate acidity during this haze episode, with median pH values in the order of 5.2 (4.8–6.9, R-PY) > 5.1 (4.7–6.5, R-AY) > 4.9 (4.1–6.8, R-XX) > 4.8 (3.9–5.9, U-AY) > 4.5 (3.8–5.2, U-ZZ). As summarized in Table 1, the $PM_{2.5}$ pH values in this work were comparable with the results found in other cities in China (e.g., Beijing, Xi'an, and Tianjin). Moreover, pH values at rural sites (i.e., R-

https://doi.org/10.5194/acp-2019-945
Preprint. Discussion started: 23 October 2019
© Author(s) 2019. CC BY 4.0 License.

Atmospheric Chemistry and Physics Discussions

207 AY, R-XX, and R-PY) were slightly higher than those at urban sites found in this and other studies.

208 The median pH values at the five sites during Case 1 (Fig. 3a) were 0.2 (U-AY)–0.9 (R-PY) pH
209 units higher than those in Case 2 (Fig. 3b). As shown in Figs. 2 and 3(d, g), pH values are closely
210 negatively correlated with H^+_{air} concentrations both in Cases 1 (r = –0.92) and 2 (r = –0.74). Moreover,
211 H^+_{air} concentrations were relevant for the total concentrations of WSIIs in Cases 1 (r = 0.73) and 2 (r
212 = 0.63). These results suggest that predicted $PM_{2.5}$ pH values were significantly affected by the WSIIs
213 levels. Similar trends were also observed in Case 3 (Figs. 3c, f, and i). However, the median pH values
214 in Case 3, which range from 4.4 (U-ZZ) to 5.3 (R-PY), were close to the pH values in Case 2 and lower
215 than those in Case 1. In reference to Section 3.1, the diversity of pH values in Cases 1 and 3 may be
216 due to the different proportions of particle- and gas-phase constituents. Table S2 shows that H^+_{air} is
217 significantly correlated with TNH_x, SO_4^{2-}, TNO_3 (NO_3^-+HNO_3), and TCl (Cl^-+HCl) at all sites
218 because of these species account for the highest proportions of total WSIIs.

219 The correlations between RH and H^+_{air} suggest the major role of RH in particle pH. In addition,
220 AWC concentration is largely determined by meteorological conditions (i.e., RH and T) (Liu et al.,
221 2017). Given the Case 2 was less affected by regional transport and could represent the local pollution
222 characteristics for distinguishing urban and rural sites better, the diurnal patterns of median pH values
223 of the five sites in this case (Fig. 4) imply that pH values were 0.3 (R-PY)–0.5 (U-ZZ) units higher
224 during nighttime than daytime. Similar results were also reported in other cities (e.g., Beijing, and
225 Tianjin) (Ding et al., 2019; Shi et al., 2019) because of the diurnal trends of T and RH (Fig. 4f) during
226 winter haze episodes in China.

https://doi.org/10.5194/acp-2019-945
Preprint. Discussion started: 23 October 2019
© Author(s) 2019. CC BY 4.0 License.

Atmospheric Chemistry and Physics Discussions

3.3 Sensitivity test of pH

The median pH values at the five sites were all in the order of R-PY > R-AY > R-XX > U-AY > U-ZZ during three cases under different pollution levels and meteorological conditions, indicating that dominant factors determine the local particle pH levels and resulting in the high pH values at rural sites. The pH sensitivity represented by the relative standard deviation (RSD) to each WSIIs and meteorological parameters (i.e., T and RH) were carried out using the average values in Case 2 (Table 3). To represent the actual ambient conditions better, the ranges of each factor near the observed minimum and maximum values in Case 2 were selected in the sensitivity tests. As shown in Figs. 5 and S6, the most important factor that influenced the predicted pH was TNH_x, followed by SO_4^{2-} and T at the five sites. The U-ZZ site was also slightly affected by TNO_3. These results are distinctly different from the results found in Beijing (SO_4^{2-} > TNH_x > TNO_3 > T in winter) (Ding et al., 2019). Similarly, RH, TCl, Na^+ and crustal ions (i.e., K^+, Ca^{2+}, and Mg^{2+}) have less influence on the predicted pH values. In general, pH values gradually grow with increased cation and decreased anion concentration though suppressing the production of H^+_{air} and AWC. Specifically, the TNH_x concentration that increased from 25 μg/m^3 to 90 μg/m^3 can promote particle pH by 3.5 (U-ZZ)–4.5 (R-AY) units. Moreover, SO_4^{2-} and TNO_3 that increased from 10 μg/m^3 to 80 μg/m^3 and 1 μg/m^3 to 125 μg/m^3 can reduce the pH values by 1.5 (R-PY)–4.0 (U-ZZ) and 0.2 (R-AY)–1.4 (U-ZZ) units, respectively. In addition, a 20 ℃ (–5 ℃ to 15 ℃) and 65% (30% to 95%) increase drops the pH by approximately 1.3 and 2.7 units at the five sites, respectively. The reason is that high T facilitated the dissociation of particle-phase ammonium (e.g., NH_4NO_3), and high RH enhanced the AWC concentration (Saraswati et al., 2019). Consequently, lower TNH_x concentrations and higher T values

https://doi.org/10.5194/acp-2019-945
Preprint. Discussion started: 23 October 2019
© Author(s) 2019. CC BY 4.0 License.

Atmospheric Chemistry and Physics Discussions

caused the lower pH values at urban sites than rural sites.

The pH values (Figs. 5 and S6) obtained from each sensitivity test at the five sites under the same conditions are nearly in the order of R-PY > R-AY > R-XX > U-AY > U-ZZ, except for the TNH_x, which is the same with the order of the median pH in Case 2 (Fig. 3b). These results imply that TNH_x dominated the local pH values in this work. However, the observed average TNH_x concentrations in Case 2 were in the order of R-AY (68.1 ± 16.6 μg/m^3) > R-PY (62.8 ± 17.9 μg/m^3) > R-XX (56.8 ± 15.7 μg/m^3) > U-AY (55.5 ± 15.2 μg/m^3) > U-ZZ (46.8 ± 14.7 μg/m^3). To gain insight into the role of TNH_x on pH, the sensitivities of pH to TNH_x at each site are illustrated in Fig. 6 with the concentrations of TNH_x, Required-NH_x, Excess-NH_x, and corresponding pH values marked. Similar growth trends of pH to increasing TNH_x are presented in Fig. 6(a). Figures 6(b-f) suggest that the calculated Excess-NH_x at the five sites significantly affected the pH values with 1.5 (U-ZZ)–2 (R-PY) units increased. Note that the order of pH values in Required-NH_x concentrations at the five sites are changed. In addition, the order of Excess-NH_x concentrations (i.e., R-PY (30.1 ± 6.2 μg/m^3) > R-AY (27.1 ± 4.2 μg/m^3) > R-XX (26.0 ± 4.6 μg/m^3) > U-AY (24.3 ± 3.9 μg/m^3)> U-ZZ (14.8 ± 4.1 μg/m^3)) is the same with the order of pH in Case 2. Therefore, Excess-NH_x concentrations during the observation periods may determine the local pH values rather than TNH_x.

Additionally, figure 6(a) shows that when the TNH_x concentrations are extremely high (> 70 μg/m^3), the pH values increase slowly and are close to 5.2, 5.4, 5.5, 5.6, and 5.6 at U-ZZ, U-AY, R-XX, R-AY, and R-PY, respectively. Similar results were reported by Guo et al., (2017) and Song et al., (2018), because NH_3 reacted with SO_4^{2-} and HNO_3 orderly, during when large amounts of H^+_{air} were consumed and pH values rapidly increased. Subsequently, dissolving NH_3 into the particles became

https://doi.org/10.5194/acp-2019-945
Preprint. Discussion started: 23 October 2019
© Author(s) 2019. CC BY 4.0 License.

Atmospheric Chemistry and Physics Discussions

difficult, and pH values slowly increased (Ding et al., 2019; Seinfeld and Pandis, 2016). These results indicate that elevated TNH_x concentrations are not sufficient in achieving a fully neutralized condition for $PM_{2.5}$. Note that the order of pH values under high TNH_x concentrations (> 70 μg/m^3) at five sites are R-PY > R-AY > R-XX > U-AY > U-ZZ, which is opposite to the order of observed T values in Case 2 with U-ZZ (5.2 ± 3.2 ℃) > U-AY (3.0 ± 3.0 ℃) > R-XX (1.9 ± 3.9 ℃) > R-AY (1.3 ± 3.2 ℃) > R-PY (1.0 ± 3.7 ℃). Therefore, T affects the content of NH_4^+ in particles and thus change H^+_{air}.

3.4 Factors that affect pH sensitivity

The sensitivities of pH to SO_4^{2-}, TNO_3, as well as other ions (except for TNH_x), at urban sites were more significant than those at rural sites, especially for U-ZZ sites with 7.2% and 14.8% of RSD to SO_4^{2-} and TNO_3, respectively. By contrast, the sensitivities of pH to TNH_x at the five sites are unordered. To further understand the major drivers, the sensitivities of pH to SO_4^{2-}, TNO_3, and TNH_x were explored using the fixed SO_4^{2-} (36.5 μg/m^3) and TNO_3 (67.5 μg/m^3) concentrations under fixed meteorological parameters (T = 2.5 ℃ and RH = 60%), of which these values are close to the average values of the five sites in Case 2 (i.e., 36.4 ± 15.4 μg/m^3 for SO_4^{2-}, 67.5 ± 23.5 μg/m^3 for TNO_3, 2.5 ± 1.5 ℃ for T, and 59.3 ±14.0% for RH). As shown in Figs. 7(a, b), the RSD values of pH to SO_4^{2-} and TNO_3 (purple lines) increase with the decrease in TNH_x concentrations (20–120 μg/m^3), especially when the TNH_x concentrations are lower than 60 μg/m^3 and 40 μg/m^3, respectively. Therefore, the sensitivities of pH to $SO_4^{2-}$and TNO_3 at the U-ZZ site were obviously higher than those of other sites with the lowest TNH_x concentrations (46.8 ± 14.7 μg/m^3). These results suggest that low ammonia determined the high sensitivities of particle pH to sulfate and nitrate at urban sites.

Good liner relations (red lines) between the RSD values of pH to TNH_x concentrations with SO_4^{2-}

https://doi.org/10.5194/acp-2019-945
Preprint. Discussion started: 23 October 2019
© Author(s) 2019. CC BY 4.0 License.

Atmospheric Chemistry and Physics Discussions

and TNO_3 concentration (1–120 μg/m^3) are observed with the following equations:

$$RSD_{A/S} = 0.0079[SO_4^{2-}] + 0.2940, \quad (6)$$

$$RSD_{A/N} = 0.0027[TNO_3] + 0.4092, \quad (7)$$

where $RSD_{A/S}$ and $RSD_{A/N}$ represent the pH sensitivities to TNH_x under different mass concentrations of SO_4^{2-} [SO_4^{2-}] and TNO_3 [TNO_3], respectively. The results show that the influence of SO_4^{2-} on the sensitivity of pH to TNH_x is roughly 2.9 times greater than that of TNO_3 in the same concentrations. The observed average TNO_3 concentrations were 1.7 (U-AY)–2.1 (R-XX) times higher than those of SO_4^{2-} at the five sites in Case 2. Moreover, the order of RSD values of pH to TNH_x (Fig. 5d) at the five sites is the same as that of the average SO_4^{2-} concentrations (Table 3). Thus, the pH sensitivities to TNH_x were dominated by SO_4^{2-} concentrations in our analysis, and the pH values were easily changeable when altering the ammonia concentration under high sulfate conditions. In the long run, recent data suggested the decreasing sulfate concentration in $PM_{2.5}$ accompanied with increasing nitrate concentration compared to earlier years during haze episodes in China, because strong actions were taken to reduce the coal consumption in recent years (Tian et al., 2017; Wang et al., 2017). Therefore, TNO_3 may rule the sensitivity of pH to TNH_x in this region at some point in the future.

3.5 Implications of regional transport

The difference in pH characteristics between Cases 1 and 2 indicates that regional transport has a remarkable influence on local particle pH. As discussed above, air mass from rural regions may increase the particle pH in urban ambient. Moreover, the sampling regions in this study are located in the transport route for Beijing (MEP, 2017), thereby contributing to the high concentrations of air pollutants. In addition, the lifetimes of NH_3 (1–5 days or less) and NH_4^+ (1–15 days) in the atmosphere

https://doi.org/10.5194/acp-2019-945
Preprint. Discussion started: 23 October 2019
© Author(s) 2019. CC BY 4.0 License.

Atmospheric Chemistry and Physics Discussions

311 are sufficient for transporting to Beijing during a haze episode (Aneja, 2000; Lefer et al., 1999;
312 Warneck, 1988). Therefore, the particle pH in Beijing will be enhanced when southern air masses
313 accompany elevated-pH particles and high ammonia levels from agricultural regions. Aqueous
314 formations of sulfate are strongly dependent on particle pH levels. Chen et al. (2016) reported that the
315 aqueous-phase sulfate production rates from NO_2 and O_3 oxidation of SO_2 had a positive correlation
316 with particle pH value during the Beijing haze events. When pH exceeded approximately 4.5 (higher
317 than this value at rural sites in this work), NO_2-oxidation dominated the sulfate formation, and its
318 reaction rate increased by one order of magnitude with the rise of pH by one unit. Thus, air masses
319 transported from rural and agricultural regions may promote sulfate formation. Therefore, ammonia
320 should be included in the regional strategy to improve air quality in China.

321 **4 Conclusions**

322 An experiment was performed using a series of high time-resolution instruments in two urban
323 (i.e., U-ZZ and U-AY) and three rural sites (i.e., R-AY, R-XX, and R-PY) in Henan Province during a
324 large-scale and long-lasting haze episode. The ISORROPIA-II model was used to investigate the pH
325 value and its driving factors. $PM_{2.5}$ exhibited moderate acidity, with median pH values in the order of
326 5.2 (4.8–6.9, R-PY) > 5.1 (4.7–6.5, R-AY) > 4.9 (4.1–6.8, R-XX)> 4.8 (3.9–5.9, U-AY)> 4.5 (3.8–5.2,
327 U-ZZ). The pH values in rural sites were slightly higher than those in urban sites.

328 The predicted pH values of $PM_{2.5}$ were significantly affected by the WSIIs levels, the different
329 proportions of particle- and gas-phase constituents, and meteorological parameters. The sensitivity
330 tests of pH values showed that TNH_x, followed by SO_4^{2-} and T, were the important factors that
331 influenced the predicted pH values at the five sites. Generally, pH values rise with the increase in

https://doi.org/10.5194/acp-2019-945
Preprint. Discussion started: 23 October 2019
© Author(s) 2019. CC BY 4.0 License.

Atmospheric Chemistry and Physics Discussions

cation increasing, and the decrease in the anion, T, and RH. The increase in TNH_x concentration from 25 μg/m^3 to 90 μg/m^3 can promote particle pH by 3.5 (U-ZZ)–4.5 (R-AY) units. Further study demonstrates that excess NH_x concentrations during observing periods determined the local pH values rather than TNH_x. In addition, ammonia determined the sensitivities of sulfate and nitrate on particle pH. Different pH sensitivities to TNH_x at the five sites were closely related to SO_4^{2-} concentrations. Therefore, air masses transported from rural and agricultural regions with elevated pH particles and high ammonia levels may promote the sulfate formation in urban aerosols. Therefore, ammonia should be involved in the regional strategy for improving the air quality in China.

Data availability. All data in this work are available by contacting the corresponding author Shasha Yin (shashayin@zzu.edu.cn)

Author contributions. Shasha Yin and Ruiqin Zhang designed and led this study. Shasha Yin was responsible for all observations and data collection. Lingling Wang, Yuping Li, Chen Wang, and Weisi Wang interpreted the data and discussed the results. Shenbo Wang wrote the paper.

Competing interests. The authors declare that they have no conflict of interest.

Acknowledgment

This work was supported by the National Key R&D Program of China (No. 2017YFC0212403) and the National Natural Science Foundation of China (No. 41907187). We thank Qi Hao and Liuming Yang for their contributions to the field observations.

https://doi.org/10.5194/acp-2019-945
Preprint. Discussion started: 23 October 2019
© Author(s) 2019. CC BY 4.0 License.

Atmospheric Chemistry and Physics Discussions

353 **References**

354 Aneja, V. P., Chauhan, J. P., Walker, J. T.: Characterization of atmospheric ammonia emissions from
355 swine waste storage and treatment lagoons. J. Geophy. Res.-Atmos., 105, 11535−11545, 2000.
356 Behera, S. N., Betha, R., Liu, P., Balasubramanian, R.: A study of diurnal variations of $PM_{2.5}$ acidity
357 and related chemical species using a new thermodynamic equilibrium model. Sci. Total Environ.,
358 452, 286−295, 2013..
359 Boucher, O., Anderson, T. L.: General circulation model assessment of the sensitivity of direct climate
360 forcing by anthropogenic sulfate aerosols to aerosol size and chemistry. J. Geophy. Res.-Atmos.,
361 100, 26117−26134, 1995.
362 Bougiatioti, A., Nikolaou, P., Stavroulas, I., Kouvarakis, G., Weber, R., Nenes, A., Kanakidou, M.,
363 Mihalopoulos, N.: Particle water and pH in the eastern Mediterranean: source variability and
364 implications for nutrient availability. Atmos. Chem. Phy., 16, 4579−4591, 2016.
365 Cheng, Y., Zheng, G., Wei, C., Mu, Q., Zheng, B., Wang, Z., Gao, M., Zhang, Q., He, K., Carmichael,
366 G.: Reactive nitrogen chemistry in aerosol water as a source of sulfate during haze events in China.
367 Sci. Adv., 2, e1601530−e1601530, 2016.
368 Clegg, S. L., Brimblecombe, P., Wexler, A. S.: The rmodynamic model of the system
369 H^+−NH_4^+−SO_4^{2-}−NO_3^-−H_2O at tropospheric temperatures. J. Phy. Chem. A, 102, 2137−2154,
370 1998.
371 Ding, J., Zhao, P., Su, J., Dong, Q., Du, X., Zhang, Y.: Aerosol pH and its driving factors in Beijing.
372 Atmos. Chem. Phy., 19, 7939−7954, 2019.
373 Dockery, D. W., Cunningham, J., Damokosh, A. L., Neas, L. M., Spengler, J. D., Koutrakis, P., Ware,

https://doi.org/10.5194/acp-2019-945
Preprint. Discussion started: 23 October 2019
© Author(s) 2019. CC BY 4.0 License.

Atmospheric Chemistry and Physics Discussions

374 J. H., Raizenne, M., Speizer, F. E.: Health effects of acid aerosols on North American children:
375 respiratory symptoms. Environ. Health Persp., 104, 500−505, 1996.
376 Guo, H., Sullivan, A. P., Campuzanojost, P., Schroder, J. C., Lopezhilfiker, F. D., Dibb, J. E., Jimenez,
377 J. L., Thornton, J. A., Brown, S. S., Nenes, A.: Fine particle pH and the partitioning of nitric acid
378 during winter in the northeastern United States. J. Geophy. Res.-Atmos., 121, 10−355, 2016.
379 Guo, H., Weber, R. J., Nenes, A.: High levels of ammonia do not raise fine particle pH sufficiently to
380 yield nitrogen oxide-dominated sulfate production. Sci. Rep., 7, 12109, 2017.
381 Guo, H., Xu, L., Bougiatioti, A., Cerully, K. M., Capps, S. L., Hite, J. R., Carlton, A. G., Lee, S., Bergin,
382 M. H., Ng, N. L.: Fine-particle water and pH in the southeastern United States. Atmos. Chem.
383 Phy., 15, 5211−5228, 2014.
384 Huang, X., Song, Y., Li, M., Li, J., Huo, Q., Cai, X., Zhu, T., Hu, M., Zhang, H.: A high-resolution
385 ammonia emission inventory in China. Global Biogeochem. Cy., 26, GB1030, 2012.
386 Larssen, T., Lydersen, E., Tang, D., He, Y., Gao, J., Liu, H., Duan, L., Seip, H .M., Vogt, R. D., Mulder,
387 J.: Acid rain in China. Environ. Sci. Technol., 40, 418−425, 2006.
388 Lefer, B. L., Talbot, R. W., Munger, J. W.: Nitric acid and ammonia at a rural northeastern US site. J.
389 Geophy. Res.-Atmos., 104, 1645−1661, 1999.
390 Li, Y. J., Sun, Y., Zhang, Q., Li, X., Li, M., Zhou, Z., Chan, C. K.: Real-time chemical characterization
391 of atmospheric particulate matter in China: A review. Atmos. Environ., 158, 270−304, 2006.
392 Liu, M., Song, Y., Zhou, T., Xu, Z., Yan, C., Zheng, M., Wu, Z., Hu, M., Wu, Y., Zhu, T.: Fine particle
393 pH during severe haze episodes in northern China. Geophys. Res. Lett., 44, 5213−5221, 2017.
394 Markovic, M. Z., Vandenboer, T. C., Murphy, J. G.: Characterization and optimization of an online

https://doi.org/10.5194/acp-2019-945
Preprint. Discussion started: 23 October 2019
© Author(s) 2019. CC BY 4.0 License.

Atmospheric Chemistry and Physics Discussions

395 system for the simultaneous measurement of atmospheric water-soluble constituents in the gas
396 and particle phases. J Environ. Monitor., 14, 1872−1884, 2012..
397 Meng, Z., Lin, W., Jiang, X., Yan, P., Wang, Y., Zhang, Y. M., Jia, X. F., Yu, X. L.: Characteristics of
398 atmospheric ammonia over Beijing, China. Atmos. Chem. Phy., 11, 6139−6151, 2011.
399 Meng, Z., Xu, X., Lin, W., Ge, B., Xie, Y., Song, B., Jia, S., Zhang, R., Peng, W., Wang, Y.: Role of
400 ambient ammonia in particulate ammonium formation at a rural site in the North China Plain.
401 Atmos. Chem. Phy., 18, 167−184, 2017.
402 MEP: 2017 air pollution prevention and management plan for the Beijing-Tianjin-Hebei region and its
403 surrounding areas, http://dqhj.mee.gov.cn/dtxx/201703/t20170323_408663.shtml (last access: 18
404 August 2019), 2017.
405 Meskhidze, N., Chameides, W. L., Nenes, A., Chen, G.: Iron mobilization in mineral dust: Can
406 anthropogenic SO_2 emissions affect ocean productivity? Geophys. Res. Lett., 30, 2003.
407 National Bureau of Statistics (NBS), 2016. China Statistical Yearbook. China Statistics Press, Beijing.
408 Accessed date: Sept. 2019.
409 Nenes, A., Pandis, S. N., Pilinis, C.: ISORROPIA: A new thermodynamic equilibrium model for
410 multiphase multicomponent inorganic aerosols. Aquat. Geochem., 4, 123−152, 1998.
411 Ostro, B., Lipsett, M., Wiener, M.B., Selner, J.C.: Asthmatic responses to airborne acid aerosols. Am.
412 J. Public Health, 81, 694−702, 1991.
413 Panteliadis, P., Hafkenscheid, T., Cary, B., Diapouli, E., Fischer, A., Favez, O., Quincey, P., Viana, M.,
414 Hitzenberger, R., Vecchi, R.: ECOC comparison exercise with identical thermal protocols after
415 temperature offset correction: instrument diagnostics by in-depth evaluation of operational

https://doi.org/10.5194/acp-2019-945
Preprint. Discussion started: 23 October 2019
© Author(s) 2019. CC BY 4.0 License.

parameters. Atmos. Meas. Tech., 8, 779−792, 2014.

Pathak, R. K., Louie, P. K., Chan, C. K.: Characteristics of aerosol acidity in Hong Kong. Atmos. Environ., 38, 2965−2974, 2004.

Rumsey, I. C., Cowen, K. A., Walker, J. T., Kelly, T. J., Hanft, E. A., Mishoe, K., Rogers, C., Proost, R., Beachley, G. M., Lear, G.: An assessment of the performance of the Monitor for AeRosols and GAses in ambient air (MARGA): a semi-continuous method for soluble compounds. Atmos. Chem. Phy., 14, 5639−5658, 2013.

Saraswati, Sharma, S. K., Saxena, M., Mandal, T. K.: Characteristics of gaseous and particulate ammonia and their role in the formation of secondary inorganic particulate matter at Delhi, India. Atmos. Res., 218, 34−49, 2019.

Seinfeld, J. H. and Pandis, S. N.: Atmospheric Chemistry and Physics: From Air Pollution to Climate Change, 2nd Edition, John Wiley and Sons, Inc., Hoboken, New Jersey, USA, 2006.

Seinfeld, J. H. and Pandis, S. N.: Atmospheric Chemistry and Physics: From Air Pollution to Climate Change (3rd edition), John Wiley and Sons, Inc., Hoboken, New Jersey, USA, 2016.

Shen, J., Liu, X., Ying, Z., Fangmeier, A., Goulding, K., Zhang, F.: Atmospheric ammonia and particulate ammonium from agricultural sources in the North China Plain. Atmos. Environ., 45, 5033−5041, 2011.

Shi, G., Xu, J., Peng, X., Xiao, Z., Chen, K., Tian, Y., Guan, X., Feng, Y., Yu, H., Nenes, A.: pH of aerosols in a polluted atmosphere: source contributions to highly acidic aerosol. Environ. Sci. Technol., 51, 4289−4296, 2017.

Shi, X., Nenes, A., Xiao, Z., Song, S., Yu, H., Shi, G., Zhao, Q., Chen, K., Feng, Y., Russell, A. G.:

https://doi.org/10.5194/acp-2019-945
Preprint. Discussion started: 23 October 2019
© Author(s) 2019. CC BY 4.0 License.

Atmospheric Chemistry and Physics Discussions

437 High-resolution data sets unravel the effects of sources and meteorological conditions on nitrate
438 and its gas-particle partitioning. Environ. Sci. Technol., 53, 3048−3057, 2019.
439 Shi, Z., Bonneville, S., Krom, M. D., Carslaw, K. S., Jickells, T. D., Baker, A. R., Benning, L. G.: Iron
440 dissolution kinetics of mineral dust at low pH during simulated atmospheric processing. Atmos.
441 Chem. Phy., 11, 995−1007, 2010.
442 Song, S., Gao, M., Xu, W., Shao, J., Shi, G., Wang, S., Wang, Y., Sun, Y., Mcelroy, M. B.: Fine particle
443 pH for Beijing winter haze as inferred from different thermodynamic equilibrium models. Atmos.
444 Chem. Phy., 18, 7423−7438, 2018.
445 Spurny, K. R.: Atmospheric acidic aerosols (review). J Aerosol Sci., 21, 1990.
446 Surratt, J. D., Chan, A. W. H., Eddingsaas, N. C., Chan, M. N., Loza, C. L., Kwan, A. J., Hersey, S.,
447 Flagan, R. C., Wennberg, P. O., Seinfeld, J. H.: Reactive intermediates revealed in secondary
448 organic aerosol formation from isoprene. P. Natl. Acad. Sci. USA., 107, 6640−6645, 2010.
449 Tao, Y. and Murphy, J. G.: The sensitivity of $PM_{2.5}$ acidity to meteorological parameters and chemical
450 composition changes: 10-year records from six Canadian monitoring sites. Atmos. Chem. Phy..
451 19, 9309−9320, 2019.
452 Tian, M., Wang, H., Chen, Y., Zhang, L., Shi, G., Liu, Y., Yu, J., Zhai, C., Wang, J., Yang, F.: Highly
453 time-resolved characterization of water-soluble inorganic ions in $PM_{2.5}$ in a humid and acidic
454 mega city in Sichuan Basin, China. Sci. Total Environ., 580, 224−234, 2017.
455 Wang, C., Yin, S., Bai, L., Zhang, X., Gu, X., Zhang, H., Lu, Q., Zhang, R.: High-resolution ammonia
456 emission inventories with comprehensive analysis and evaluation in Henan, China, 2006–2016.
457 Atmos. Environ., 193, 11−23, 2018a.

https://doi.org/10.5194/acp-2019-945
Preprint. Discussion started: 23 October 2019
© Author(s) 2019. CC BY 4.0 License.

458 Wang, G., Zhang, F., Peng, J., Duan, L., Ji, Y., Marreroortiz, W., Wang, J., Li, J., Wu, C., Cao, C.:
459 Particle acidity and sulfate production during severe haze events in China cannot be reliably
460 inferred by assuming a mixture of inorganic salts. Atmos. Chem. Phy., 18, 1−23, 2018b.
461 Wang, G., Zhang, R., Gomez, M. E., Yang, L., Levy, Z. M., Hu, M., Lin, Y., Peng, J., Guo, S., Meng,
462 J.: Persistent sulfate formation from London Fog to Chinese haze. P. Natl. Acad. Sci. USA., 113,
463 13630−13635, 2016.
464 Wang, H., Ding, J., Xu, J., Wen, J., Han, J., Wang, K., Shi, G., Feng, Y., Ivey, C., Wang, Y.: Aerosols
465 in an arid environment: The role of aerosol water content, particulate acidity, precursors, and
466 relative humidity on secondary inorganic aerosols. Sci. Total Environ., 646, 564−572, 2019a.
467 Wang, J., Zhao, B., Wang, S., Yang, F., Xing, J., Morawska, L., Ding, A., Kulmala, M., Kerminen, V.,
468 Kujansuu, J.: Particulate matter pollution over China and the effects of control policies. Sci. Total
469 Environ., 584, 426−447, 2017.
470 Wang, S., He, B., Yuan, M., Su, F., Yin, S., Yan, Q., Jiang, N., Zhang, R., Tang, X.: Characterization
471 of individual particles and meteorological conditions during the cold season in Zhengzhou using
472 a single particle aerosol mass spectrometer. Atmos. Res., 219, 13−23, 2019b.
473 Wang, S., Yan, Q., Yu, F., Wang, Q., Yang, L., Zhang, R., Yin, S., Wang, S., Yan, Q., Yu, F.: Distribution
474 and source of chemical elements in size-resolved particles in Zhengzhou, China: Effects of
475 regional transport. Aerosol Air Qual. Res., 18, 371−385, 2018c.
476 Wang, S., Yin, S., Zhang, R., Yang, L., Zhao, Q., Zhang, L., Yan, Q., Jiang, N., Tang, X.: Insight into
477 the formation of secondary inorganic aerosol based on high-time-resolution data during haze
478 episodes and snowfall periods in Zhengzhou, China. Sci. Total Environ., 660, 47−56, 2019c.

https://doi.org/10.5194/acp-2019-945
Preprint. Discussion started: 23 October 2019
© Author(s) 2019. CC BY 4.0 License.

Atmospheric Chemistry and Physics Discussions

479 Warneck, P.: Chemistry of the Natural Atmosphere, Academic Press, San Diego, CA, 1988.

480 Watson, J. G.: Visibility: science and regulation. J Air Waste Manage., 52, 973−999, 2002.

481 Wen, L., Chen, J., Yang, L., Wang, X., Xu, C., Sui, X., Yao, L., Zhu, Y., Zhang, J., Zhu, T.: Enhanced

482 formation of fine particulate nitrate at a rural site on the North China Plain in summer: The

483 important roles of ammonia and ozone. Atmos. Environ., 101, 294−302, 2015.

https://doi.org/10.5194/acp-2019-945
Preprint. Discussion started: 23 October 2019
© Author(s) 2019. CC BY 4.0 License.

Atmospheric Chemistry and Physics Discussions

Figure lists:

Fig. 1 Temporal variations of temperature (T), relative humidity (RH), wind speed (WS), wind direction (WD), and concentrations of NH_3 and water-soluble inorganic ions (WSIIs) in three cases at the Zhengzhou (U-ZZ) site.

Fig. 2 Time series and box plot of predicted $PM_{2.5}$ pH, H^+_{air}, and aerosol water content (AWC) at the five sites. In each box, the top, middle and bottom lines represent the 75th, 50th, and 25th percentile of statistical data, respectively; the upper and lower whiskers represent the maximum and minimum values, respectively.

Fig. 3 (a)–(c) Box plots of $PM_{2.5}$ pH at the five sites in three cases. (d)–(f) Correlations between pH and H^+_{air}. (g)–(i) Correlations between total concentrations of WSIIs and H^+_{air}. The color scale bar represents AWC concentration.

Fig. 4 (a)–(e) Diurnal patterns of median (min–max) pH values, (f) average RH, and T of the five sites in Case 2. The upper and lower ends of the line represent the maximum and minimum values of pH, respectively. The color scale bar represents AWC concentration.

Fig. 5 Sensitivity tests of $PM_{2.5}$ pH to T, RH, TCl (Cl^- + HCl), TNH_x (NH_4^+ + NH_3), TNO_3 (NO_3^- + HNO_3), and SO_4^{2-}. The range of the x-axis is close to the observed minimum and maximum values in Case 2. The color scale bar represents the pH values. The square plots on the graph represent the average values of each factor observed in Case 2 with standard deviation as an error bar. The relative standard deviation (RSD) and range (Range) represent the variation degree and range (min–max) of the pH values in the test.

Fig. 6 Sensitivity tests of $PM_{2.5}$ pH to TNH_x at the five sites. The concentrations of TNH_x, required

https://doi.org/10.5194/acp-2019-945
Preprint. Discussion started: 23 October 2019
© Author(s) 2019. CC BY 4.0 License.

Atmospheric Chemistry and Physics Discussions

505 NH_x (Required-NH_x), excess NH_x (Excess-NH_x), and corresponding pH values are plotted. The blue
506 and orange background colors correspond to the NH_x-poor and NH_x-rich, respectively.
507 Fig. 7 pH calculated with fixed meteorological parameters (T = 275.5 K and RH = 60%) under
508 different combinations of TNH_x and (a) SO_4^{2-} (Fixed TNO_3 = 67.5 μg/m^3) and (b) TNO_3 (Fixed
509 SO_4^{2-} = 36.5 μg/m^3). The color scale bar represents the pH values. The red lines in (a) and (b)
510 represent the RSD of pH for TNH_x under different SO_4^{2-} and TNO_3 concentrations, respectively, and
511 the purple lines represent the RSD of pH for SO_4^{2-} and TNO_3 in (a) and (b) under different TNH_x
512 concentrations. The markers on the graph represent the average concentrations of TNH_x, SO_4^{2-}, and
513 TNO_3 at the five sites in Case 2 with standard deviation as error bar.
514
515
516
517
518
519
520
521

https://doi.org/10.5194/acp-2019-945
Preprint. Discussion started: 23 October 2019
© Author(s) 2019. CC BY 4.0 License.

Atmospheric Chemistry and Physics Discussions

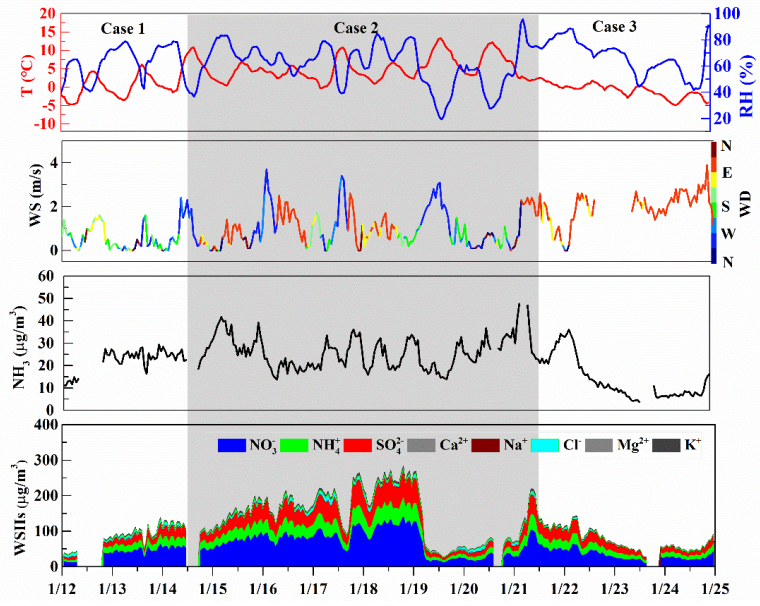

Fig. 1 Temporal variations of temperature (T), relative humidity (RH), wind speed (WS), wind direction (WD), and concentrations of NH_3 and water-soluble inorganic ions (WSIIs) in three cases at the Zhengzhou (U-ZZ) site.

https://doi.org/10.5194/acp-2019-945
Preprint. Discussion started: 23 October 2019
© Author(s) 2019. CC BY 4.0 License.

Atmospheric Chemistry and Physics Discussions

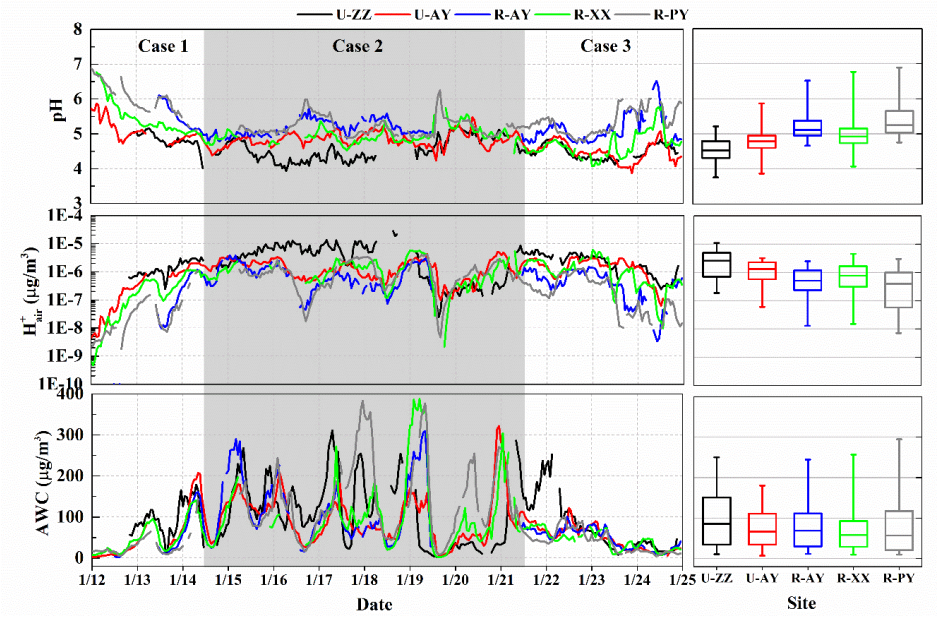

Fig. 2 Time series and box plot of predicted $PM_{2.5}$ pH, H^+_{air}, and aerosol water content (AWC) at the five sites. In each box, the top, middle and bottom lines represent the 75th, 50th, and 25th percentile of statistical data, respectively; the upper and lower whiskers represent the maximum and minimum values, respectively.

https://doi.org/10.5194/acp-2019-945
Preprint. Discussion started: 23 October 2019
© Author(s) 2019. CC BY 4.0 License.

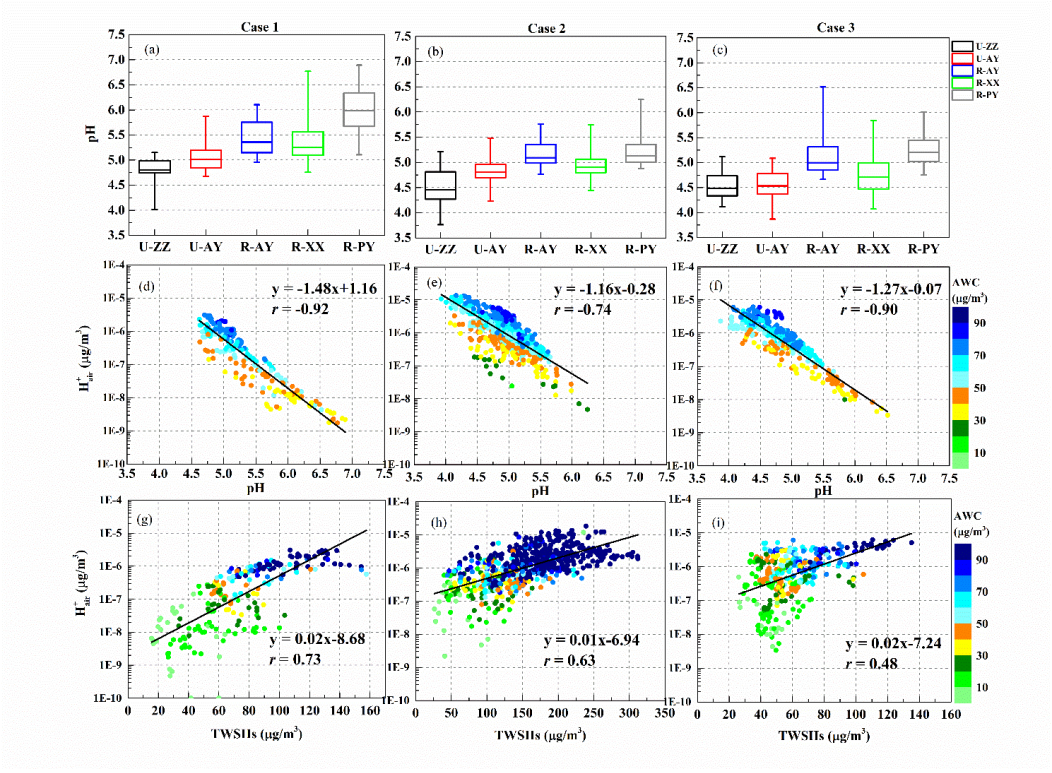

534

535 Fig. 3 (a)–(c) Box plots of $PM_{2.5}$ pH at the five sites in three cases. (d)–(f) Correlations between pH

536 and H^+_{air}. (g)–(i) Correlations between total concentrations of WSIIs and H^+_{air}. The color scale bar

537 represents AWC concentration.

538

https://doi.org/10.5194/acp-2019-945
Preprint. Discussion started: 23 October 2019
© Author(s) 2019. CC BY 4.0 License.

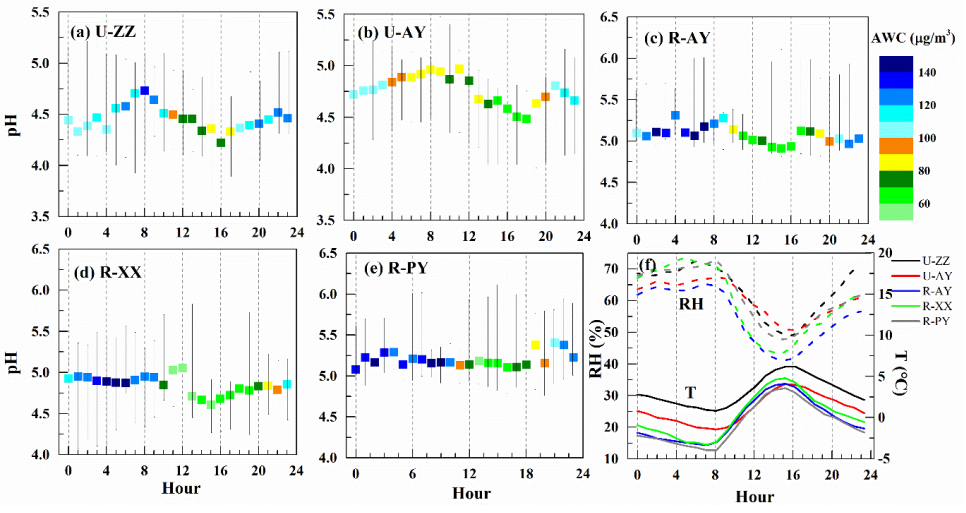

539

540 Fig. 4 (a)–(e) Diurnal patterns of median pH values, (f) average RH, and T of the five sites in Case 2.

541 The upper and lower ends of the line represent the maximum and minimum values of pH,

542 respectively. The color scale bar represents AWC concentration.

543

544

545

546

https://doi.org/10.5194/acp-2019-945
Preprint. Discussion started: 23 October 2019
© Author(s) 2019. CC BY 4.0 License.

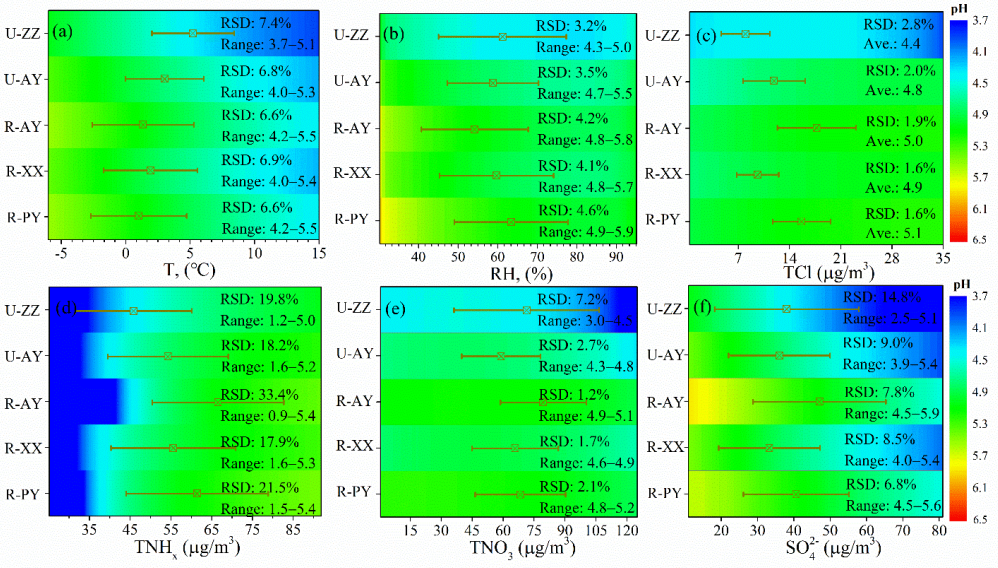

Fig. 5 Sensitivity tests of $PM_{2.5}$ pH to T, RH, TCl (Cl^- + HCl), TNH_x (NH_4^+ + NH_3), TNO_3 (NO_3^- + HNO_3), and SO_4^{2-}. The range of the x-axis is close to the observed minimum and maximum values in Case 2. The color scale bar represents the pH values. The square plots on the graph represent the average values of each factor observed in Case 2 with standard deviation as an error bar. The relative standard deviation (RSD) and range (Range) represent the variation degree and range (min–max) of the pH values in the test.

https://doi.org/10.5194/acp-2019-945
Preprint. Discussion started: 23 October 2019
© Author(s) 2019. CC BY 4.0 License.

Atmospheric Chemistry and Physics Discussions

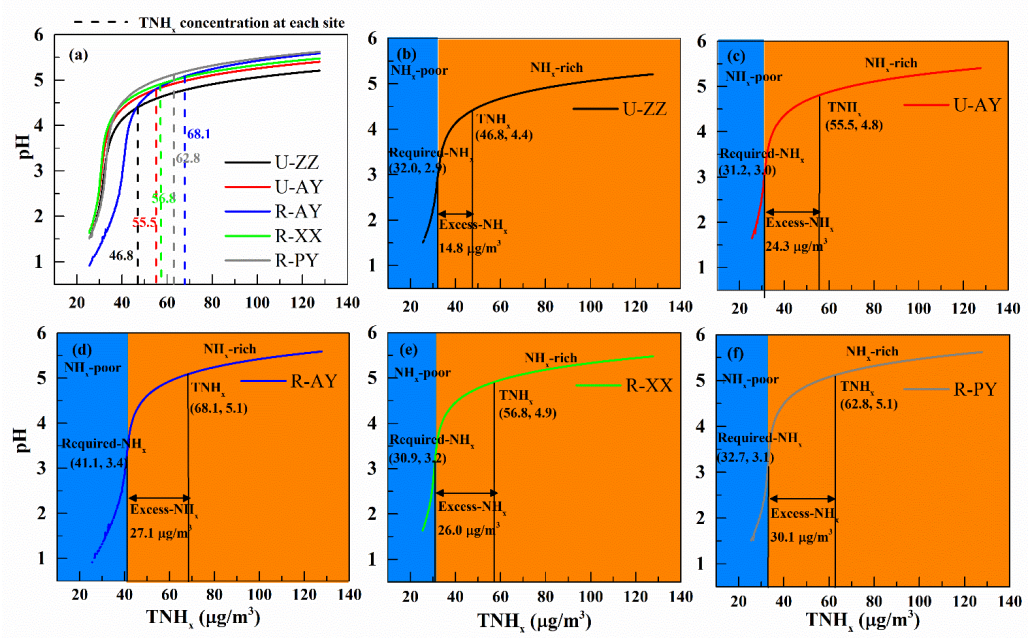

Fig. 6 Sensitivity tests of $PM_{2.5}$ pH to TNH_x at the five sites. The concentrations of TNH_x, required NH_x (Required-NH_x), excess NH_x (Excess-NH_x), and corresponding pH values are plotted. The blue and orange background colors correspond to the NH_x-poor and NH_x-rich, respectively.

https://doi.org/10.5194/acp-2019-945
Preprint. Discussion started: 23 October 2019
© Author(s) 2019. CC BY 4.0 License.

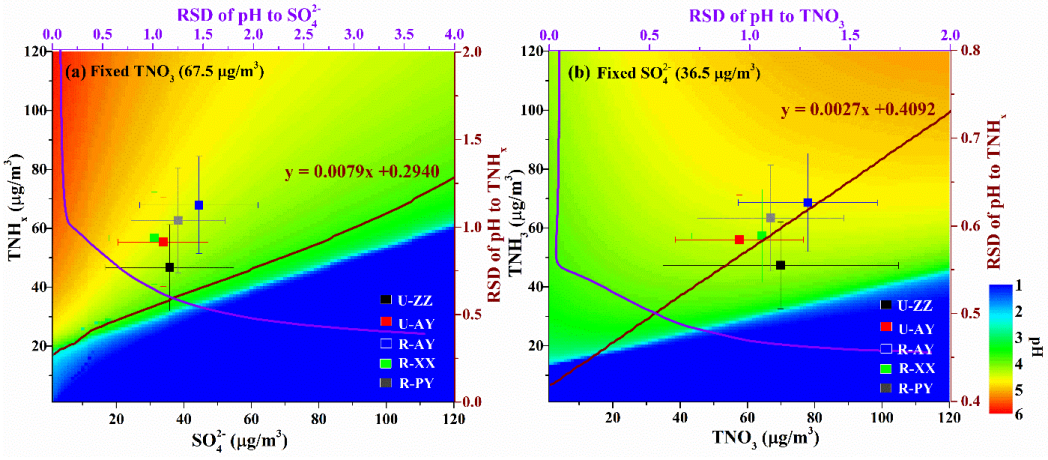

563

564 Fig. 7 pH calculated with fixed meteorological parameters (T = 275.5 K and RH = 60%) under
565 different combinations of TNH_x and (a) SO_4^{2-} (Fixed TNO_3 = 67.5 μg/m^3) and (b) TNO_3 (Fixed
566 SO_4^{2-} = 36.5 μg/m^3). The color scale bar represents the pH values. The red lines in (a) and (b)
567 represent the RSD of pH for TNH_x under different SO_4^{2-} and TNO_3 concentrations, respectively, and
568 the purple lines represent the RSD of pH for SO_4^{2-} and TNO_3 in (a) and (b) under different TNH_x
569 concentrations. The markers on the graph represent the average concentrations of TNH_x, SO_4^{2-}, and
570 TNO_3 at the five sites in Case 2 with standard deviation as error bar.

https://doi.org/10.5194/acp-2019-945
Preprint. Discussion started: 23 October 2019
© Author(s) 2019. CC BY 4.0 License.

Table lists:

Table 1 Comparison of the particle pH values in this study (median, min–max) and other sites (mean ± standard deviation).

Table 2 Descriptions of the five sampling sites.

Table 3 Summary (mean ± standard deviation) of gaseous precursors (μg/m^3), water-soluble inorganic ions (μg/m^3), temperature (°C), and relative humidity (%) during three cases of haze periods at five monitoring sites.

Atmospheric Chemistry and Physics Discussions
Open Access
EGU

https://doi.org/10.5194/acp-2019-945
Preprint. Discussion started: 23 October 2019
© Author(s) 2019. CC BY 4.0 License.

584 Table 1 Comparison of the particle pH values in this study (median, min–max) and other sites (mean ± standard deviation).

	Observation site	Period	pH	Model	Reference
This study	Zhengzhou, China (Urban)	Jan 2018	4.5 (3.8–5.2)		
	Anyang, China (Urban)	Jan 2018	4.8 (3.9–5.9)		
	Anyang, China (Rural)	Jan 2018	4.9 (4.1–6.8)	ISORROPIA-II	
	Xinxiang, China (Rural)	Jan 2018	5.1 (4.7–6.5)		
	Puyang, China (Rural)	Jan 2018	5.2 (4.8–6.9)		
China	Beijing, China (Urban)	Feb 2017	4.5 ± 0.7	ISORROPIA-II	Ding et al., 2019
	Beijing, China (Urban)	Dec 2016	4.3 ± 0.4	ISORROPIA-II	Liu et al., 2017
	Beijing, China (Urban)	Jan–Feb 2015	4.5	ISORROPIA-II	Guo et al., 2017
	Xi'an, China (Urban)	Nove–Dec 2012	5.0	ISORROPIA-II	Guo et al., 2017
	Tianjin, China (Urban)	Dec–Jun 2015	4.9 ± 1.4	ISORROPIA-II	Shi et al., 2017
	Tianjin, chain (Urban)	Aug 2015	3.4 ± 0.5	ISORROPIA-II	Shi et al., 2019
	Hohhot, China	Winter 2015	5.7	ISORROPIA-II	Wang et al., 2019
	PRD, China (Rural)	Fall-winter season 2012	0.81 ± 0.24	AIM-II model	Fu et al., 2015
	Hong Kong, China (Urban)	2001	0.25	AIM-II model	Pathak et al., 2004
Other countries	Singapore (Urban)	Sep–Nov 2011	0.60	AIM-IV model	Sailesh et al., 2013
	Northeastern United States (Urban)	Feb–Mar 2015	0.07 ± 0.96	ISORROPIA-II	Guo et al., 2016
	Alabama, USA (Rural)	Jun–Jul 2013	1.94 ± 0.59	ISORROPIA-II	Guo et al., 2015
	Crete, Greece (Background)	Aug–Nov 2012	1.25 ± 1.14	ISORROPIA-II	Boucher et al., 2016

585

Atmospheric Chemistry and Physics Discussions
Open Access
EGU

https://doi.org/10.5194/acp-2019-945
Preprint. Discussion started: 23 October 2019
© Author(s) 2019. CC BY 4.0 License.

586

587 Table 2 Descriptions of five sampling sites.

Classification	Site	Coordinate	Location	Surrounding environment
Urban	U-ZZ	34.82° N 113.54° E	West to the Zhengzhou downtown (Zhengzhou University)	Densely occupied residences, light industry, freeways and roads
Urban	U-AY	36.09° N 114.41° E	East to the Anyang downtown (Anyang Environmental Protection Bureau)	Occupied residences, heavy industry and traffic roads
Rural	R-AY	36.22° N 114.39° E	15 km north of Anyang city (Baizhuang town)	High ways, small villages, and cropland
Rural	R-XX	35.38° N 114.30° E	35 km northeast of Xinxiang city (Banzao town)	Small villages and cropland
Rural	R-PY	36.15° N 115.10° E	44 km north of Puyang city (Liangcun town)	Small villages and cropland

588

589

590

591

592

593

Atmospheric Chemistry and Physics Discussions
Open Access
EGU

https://doi.org/10.5194/acp-2019-945
Preprint. Discussion started: 23 October 2019
© Author(s) 2019. CC BY 4.0 License.

Table 3 Summary (mean ± standard deviation) of gaseous precursors (μg/m^3), water-soluble inorganic ions (μg/m^3), temperature (°C), and relative humidity (%) during three cases of haze periods at five sites.

	Case 1 (January 12−14)					Case 2 (January 14−21)					Case 3 (January 21−25)				
	U-ZZ	U-AY	R-AY	R-XX	R-PY	U-ZZ	U-AY	R-AY	R-XX	R-PY	U-ZZ	U-AY	R-AY	R-XX	R-PY
HNO_3	0.9 ± 0.2	0.7 ± 0.2	3.1 ± 0.2	3.0 ± 0.1	3.9 ± 0.1	1.3 ± 0.3	1.1 ± 0.3	3.7 ± 0.4	3.7 ± 0.5	4.2 ± 0.2	0.9 ± 0.3	0.7 ± 0.2	4.9 ± 1.0	3.3 ± 0.2	3.3 ± 0.2
NH_3	17.0 ± 3.7	19.6 ± 8.0	22.9 ± 6.3	21.6 ± 4.1	17.8 ± 3.7	19.0 ± 5.3	23.1 ± 6.6	25.0 ± 6.7	25.1 ± 10.0	26.5 ± 6.7	10.5 ± 6.9	8.8 ± 4.7	10.6 ± 4.7	8.4 ± 3.5	12.1 ± 3.5
HCl	0.1 ± 0.0	0.7 ± 0.6	0.5 ± 0.1	0.6 ± 0.1	1.8 ± 0.1	0.2 ± 0.3	0.5 ± 0.2	0.6 ± 0.2	0.6 ± 0.1	2.0 ± 0.2	0.1 ± 0.1	0.5 ± 0.1	1.7 ± 0.1	1.0 ± 0.4	1.5 ± 0.4
NO_3^-	41.5 ± 14.6	28.0 ± 14.6	43.0 ± 12.5	32.8 ± 12.9	25.2 ± 9.1	68.8 ± 34.9	56.6 ± 19.0	74.5 ± 20.7	60.8 ± 20.7	63.0 ± 21.6	32.4 ± 13.5	18.9 ± 5.4	26.0 ± 5.8	25.1 ± 6.7	18.8 ± 4.3
NH_4^+	18.6 ± 6.2	15.9 ± 8.3	21.8 ± 8.0	14.9 ± 6.2	12.8 ± 4.5	29.5 ± 13.6	34.3 ± 12.5	45.5 ± 13.6	33.0 ± 11.7	38.7 ± 15.0	17.4 ± 6.0	11.6 ± 4.4	14.3 ± 4.4	12.9 ± 4.0	10.1 ± 2.9
SO_4^{2-}	17.8 ± 7.2	14.4 ± 9.0	18.1 ± 10.0	10.0 ± 5.5	8.6 ± 2.3	35.5 ± 19.0	33.5 ± 13.4	44.1 ± 17.5	30.9 ± 13.4	38.0 ± 13.9	19.8 ± 8.6	15.1 ± 6.1	15.1 ± 7.3	14.4 ± 4.8	13.3 ± 4.0
Ca^{2+}	0.7 ± 0.5	0.5 ± 0.3	5.0 ± 2.2	0.8 ± 0.2	3.4 ± 0.3	0.4 ± 0.4	0.4 ± 0.4	2.2 ± 1.1	1.0 ± 0.3	3.3 ± 0.6	0.1 ± 0.1	0.2 ± 0.2	1.8 ± 0.7	0.5 ± 0.1	2.4 ± 0.5
Na^+	1.5 ± 0.2	1.0 ± 0.0	1.4 ± 0.4	0.7 ± 0.1	2.2 ± 0.1	1.5 ± 0.2	1.0 ± 0.1	1.3 ± 0.4	0.8 ± 0.1	2.2 ± 0.0	1.1 ± 0.2	1.0 ± 0.2	2.2 ± 0.4	1.3 ± 0.4	2.2 ± 0.2
Cl^-	7.5 ± 2.5	2.7 ± 3.4	6.6 ± 2.5	5.4 ± 1.5	6.3 ± 1.2	7.9 ± 3.5	11.6 ± 4.4	17.4 ± 5.6	9.2 ± 2.9	13.9 ± 4.1	3.3 ± 1.5	4.5 ± 1.6	6.9 ± 1.6	4.7 ± 0.9	5.4 ± 1.4
Mg^{2+}	0.2 ± 0.0	0.1 ± 0.0	0.4 ± 0.1	0.1 ± 0.0	0.5 ± 0.0	0.2 ± 0.0	0.1 ± 0.0	0.4 ± 0.4	0.1 ± 0.0	0.5 ± 0.1	0.2 ± 0.0	0.1 ± 0.0	0.4 ± 0.1	0.1 ± 0.1	0.4 ± 0.1
K^+	2.9 ± 0.7	1.4 ± 0.5	1.6 ± 0.6	1.6 ± 0.4	2.5 ± 0.6	4.1 ± 1.9	2.3 ± 0.8	2.8 ± 0.7	1.8 ± 0.6	3.6 ± 1.2	1.9 ± 0.7	0.9 ± 0.3	0.8 ± 0.3	0.8 ± 0.2	1.2 ± 0.4
T	0.3 ± 3.1	−0.9 ± 3.7	−1.8 ± 4.4	−2.0 ± 3.9	−1.7 ± 4.8	5.2 ± 3.2	3.0 ± 3.0	1.3 ± 3.9	1.9 ± 3.6	1.0 ± 3.7	−0.8 ± 1.8	−2.7 ± 1.8	−3.2 ± 1.9	−2.8 ± 2.6	−4 ± 2.3
RH	63.7 ± 12.1	60.3 ± 15.4	54.0 ± 16.0	58.5 ± 13.5	49.7 ± 14.5	61.0 ± 16.1	58.6 ± 11.5	54.0 ± 13.5	59.5 ± 14.4	63.3 ± 14.3	67 ± 13.1	63.7 ± 13.8	55.9 ± 13.6	59 ± 13.7	56.8 ± 16

Atmospheric Chemistry and Physics Discussions
Open Access
EGU